
4D-GSW: Kinematic-Aware Spatio-Temporal Consistent Watermarking for 4D Gaussian Splatting

Sifan Zhou^{1†}, Hang Zhang^{2†}, Yuhang Wang³, Ming Li^{2*}

¹Southeast University

²Guangdong Laboratory of Artificial Intelligence and Digital Economy (SZ)

³University of Chinese Academy of Sciences

[†]These authors contributed equally. ^{*}Corresponding author.
sifanjay@gmail.com, liming@gml.ac.cn

Abstract

While 4D Gaussian Splatting (4DGS) has revolutionized high-fidelity dynamic reconstruction, safeguarding the intellectual property of these assets remains an open challenge. Conventional steganographic techniques often neglect the underlying kinematic manifolds, triggering non-physical artifacts such as severe temporal flickering and "FVD collapse". To address this, we propose **4D-GSW**, a kinematic-aware watermarking framework designed to embed robust copyright information while preserving high spatio-temporal consistency. Unlike prior 4D steganography that primarily focuses on opacity-guided invisibility, our approach explicitly addresses the physical coherence of motion trajectories. We introduce a **Spatio-Temporal Curvature (STC)** metric to identify "Dynamic Instants," adaptively gating watermark gradient injection to shield critical motion manifolds from non-physical perturbations. To ensure global coherence across complex deformations, we formulate a joint **HMM-MRF energy minimization** model that synchronizes watermark phases within both temporal trajectories and spatial neighborhoods. Furthermore, an **anisotropic gradient routing** mechanism ensures that watermark embedding remains strictly decoupled from photometric reconstruction fidelity. Extensive experiments have demonstrated the superior performance of our method in robustly hiding watermarks while resisting various attacks and maintaining high rendering quality and spatiotemporal consistency.

1 Introduction

Novel View Synthesis (NVS) is a crucial task in computer vision and robotics, with wide applications in autonomous driving and augmented reality. 3D Gaussian Splatting (3DGS)[15, 34] has established itself as a prominent technique in 3D rendering, offering superior quality and fast rendering speeds. The 4D extensions of 3D-GS have demonstrated significant success in effectively reconstructing complex dynamic scenes[10, 5]. The proliferation of 4D Gaussian Splatting (4D-GS) [36] has revolutionized the creation of high-fidelity dynamic digital assets, which now serve as cornerstones in autonomous driving simulation, virtual production, and telepresence [38, 6, 14, 43]. However, the immense commercial value of these assets—derived from costly multi-view acquisitions and massive compute—is starkly contrasted by their inherent vulnerability to intellectual property (IP) infringement. Unlike implicit representations, the explicit parameterized nature of 4D-GS allows attackers to easily extract, redistribute, or maliciously manipulate motion trajectories and radiance attributes [39]. Without robust and invisible copyright authentication, the large-scale deployment of these 4D assets remains high-risk, necessitating the development of specialized digital watermarking for dynamic neural rendering.

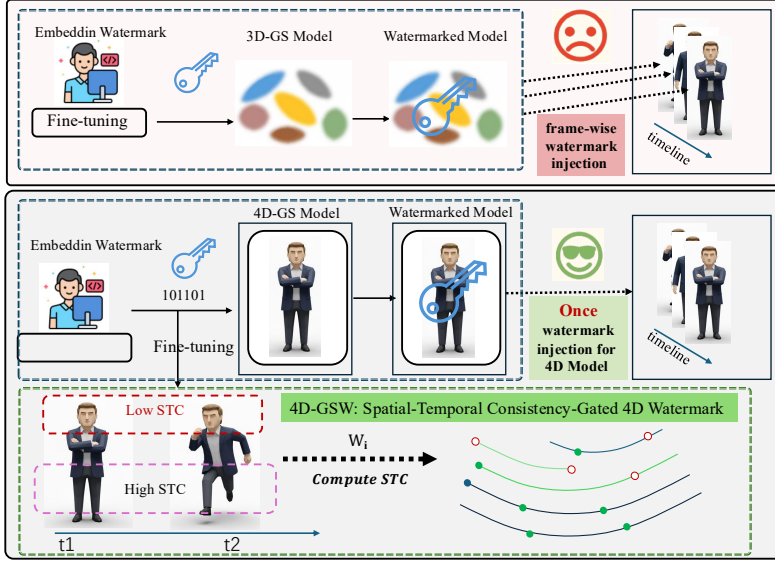


Figure 1: **Watermark framework comparison.** (**Upper**) Conventional 3D-GS watermarking schemes necessitate independent fine-tuning for each individual frame in a dynamic sequence. (**Bottom**) Our 4D-GSW treats the 4D asset as a holistic kinematic manifold. By computing the Spatio-Temporal Curvature (STC) of Gaussian trajectories, we adaptively gate the watermark gradients—prioritizing stable regions while shielding "Dynamic Instants" from non-physical perturbations.

Despite the maturity of watermarking for 2D images and 3D meshes, extending these protections to 4DGS reveals a significant technical gap. A naive migration of static 3D-GS watermarking schemes to the temporal domain fails to account for the continuous spatio-temporal manifold structure of dynamic scenes [46, 11, 7, 18]. Specifically, injecting independent watermark perturbations into each frame disrupts the physical coherence of object trajectories, leading to "FVD collapse" characterized by severe temporal flickering and geometric jitter [32, 41, 29]. While recent steganographic attempts like Hide-in-Motion [18] achieve information hiding, they primarily focus on visibility and lack explicit constraints on the underlying motion kinematics, often sacrificing spatio-temporal consistency under complex non-rigid deformations [13, 41].

To bridge this gap, we propose **4D-GSW**, a kinematic-aware watermarking framework designed to reconcile the conflict between robust data embedding and 4D physical consistency. Our core design is rooted in the intrinsic manifold of motion: we observe that watermark-induced artifacts are most prominent at "Dynamic Instants" where trajectories exhibit high Spatio-Temporal Curvature (STC). By mathematically quantifying this curvature, we introduce an adaptive gating mechanism that shields these fragile motion segments from non-physical watermark gradients [42]. To ensure the persistent and coherent distribution of the watermark field, we formulate the embedding as a *Maximum A Posteriori* (MAP) inference problem on a dynamic random field. Specifically, we integrate an *Optimal Transport* (OT) alignment module to resolve the correspondence ambiguity caused by Gaussian densification and pruning, coupled with a joint HMM-MRF energy model for global coherence. We theoretically demonstrate that this formulation is equivalent to solving an anisotropic diffusion-reaction *Partial Differential Equation* (PDE), where the watermark signal naturally flows along stable radiance manifolds while being repelled by high-dynamic boundaries. Combined with an **anisotropic gradient routing** mechanism, our method ensures that high-bitrate copyright information is "baked" into the 4D asset with high-fidelity FVD degradation. The core contributions are summarized as follows:

- **4D-GSW Framework:** We propose 4D-GSW, a kinematic-aware framework that bridges the gap between 4D asset protection and spatio-temporal consistency. As we all know, it is the first work to explicitly mitigate "FVD collapse" by aligning watermark embedding with 4D motion physics.
- **STC Gating Mechanism:** We introduce a **Spatio-Temporal Curvature (STC)** gating strategy that quantifies trajectory instability to adaptively shield "Dynamic Instants" from perturbations, preserving the integrity of complex non-rigid motions.

- **Topology-Aware Consistency:** We develop a joint **HMM-MRF** energy model integrated with Optimal Transport (OT). This resolves correspondence ambiguity during Gaussian resampling, enforcing rigorous temporal phase-locking and spatial coherence.
- **Anisotropic Diffusion Theory:** We establish a mathematical foundation by proving our curvature-gated optimization induces a steady-state solution to an Anisotropic Diffusion PDE, implemented via a gradient routing mechanism to decouple embedding from fidelity.

2 Related Work

Dynamic Scene Rendering and Watermarking. While 4D Gaussian Splatting (4DGS) and its sparse-controlled variants (e.g., SC4D [37]) enable high-fidelity dynamic scene rendering, safeguarding their intellectual property remains an open challenge. Existing neural watermarking strategies primarily target static NeRFs or 3DGS [21, 7, 9, 17, 46, 47]. Applying these static methods frame-by-frame to 4DGS invariably induces severe temporal discontinuity and structural instability. Furthermore, the only existing 4D steganography approach, Hide-in-Motion [18], relies on opacity heuristics without explicit modeling of the underlying motion physics, resulting in FVD degradation under complex non-rigid deformations. Since human perception is highly sensitive to abrupt motion changes—which can be mathematically localized via Spatio-Temporal Curvature (STC) [27]—naïve spatial embedding is inadequate. Motivated by this, our work introduces kinematic-aware priors via STC to achieve temporally consistent and imperceptible 4D copyright embedding.

3 Preliminaries

3D Gaussian Splatting. 3D Gaussian Splatting (3D-GS) [15] represents a static scene as a set of N anisotropic Gaussian ellipsoids $\mathcal{G} = \{\mathbf{g}_i\}_{i=1}^N$. Each Gaussian is defined by its center position (mean) $\boldsymbol{\mu}_i \in \mathbb{R}^3$, an opacity $\alpha_i \in [0, 1]$, and a 3D covariance matrix $\boldsymbol{\Sigma}_i$. Generally, $\boldsymbol{\Sigma}_i$ is decomposed into a scaling factor $\boldsymbol{\sigma}_i \in \mathbb{R}^3$ and a rotation quaternion $\mathbf{q}_i \in \mathbb{R}^4$. Besides, view-dependent color is encoded via spherical harmonic (SH) coefficients \mathbf{h}_i . During rendering, the pixel color $\hat{\mathbf{C}}(\mathbf{r})$ is computed through alpha compositing:

$$\hat{\mathbf{C}}(\mathbf{r}) = \sum_{k=1}^K \mathbf{c}_k \alpha_k G'_k(\mathbf{r}) \prod_{l=1}^{k-1} (1 - \alpha_l G'_l(\mathbf{r})), \quad (1)$$

where \mathbf{c}_k is the color decoded from \mathbf{h}_k and $G'_k(\mathbf{r})$ is the projected 2D Gaussian influence at pixel \mathbf{r} .

4D Gaussian Splatting. Our watermarking framework is designed to be highly generalizable across various 4D-GS backbones that model temporal dynamics[20, 36]. At any given timestamp t , the dynamic scene is represented by a set of appearance-augmented Gaussians \mathcal{P}_t :

$$\mathcal{P}_t = \{\mathbf{p}_i^t = (\mathbf{x}_i^t, \mathbf{q}_i^t, \alpha_i^t, \mathbf{s}_i^t)\}_{i=1}^N, \quad (2)$$

where \mathbf{x}_i^t and \mathbf{q}_i^t denote the time-varying spatial coordinates and rotation state, respectively. To resolve naming conflicts with the geometric scaling factor $\boldsymbol{\sigma}$, we explicitly denote \mathbf{s}_i^t as the **appearance state** (instantiated as the 0-th order Direct Current (DC) component of the SH coefficients). α_i^t denote the opacity. For notation simplicity in the subsequent optimization framework, we define $\mathbf{z}_i^t = [\mathbf{x}_i^t, \mathbf{s}_i^t]^\top$ as the coupled spatio-temporal state of the i -th Gaussian, representing its geometric center and appearance attribute, respectively. In our methodology, \mathbf{s}_i^t serves as the primary carrier for watermark signal injection, as it directly influences the radiometric output while remaining decoupled from the kinematic deformation modeling.

3.1 Problem Formulation

The objective of our framework is to embed a robust, imperceptible, and omnidirectional watermark signal into a dynamic 4DGS asset [37]. Unlike prior 4D steganography works that may rely on specific "check viewpoints" for information recovery, our task is to ensure that the watermark is recoverable from any arbitrary perspective in 360° space, effectively "baking" the copyright information into the 4D radiance field.

Watermark Encoding and Embedding. Let $\mathbf{B} \in \{0, 1\}^L$ be a binary watermark sequence of length L (e.g., $L = 48$). The embedding process is formulated as a strategic modulation of the appearance manifold $\mathcal{S} = \{\mathbf{s}_i^t\}_{i,t}$ across the temporal sequence. We define an embedding function Ψ that modifies the 0-th order SH coefficients:

$$\hat{\mathbf{s}}_i^t = \Psi(\mathbf{s}_i^t, \mathbf{B}, w_i^t), \quad (3)$$

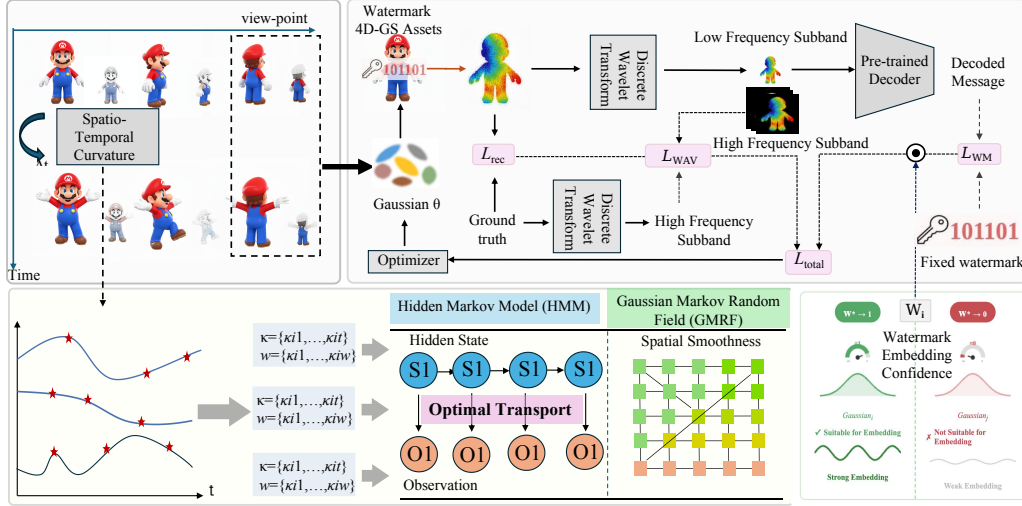


Figure 2: **4D-GSW framework overview.** Our pipeline extracts Spatio-Temporal Curvature (STC) from Gaussian trajectories to derive an embedding confidence weight. This weight guides a kinematic-aware optimization that adaptively modulates watermark gradients, prioritizing stable radiance manifolds while shielding dynamic instants. The field is further regularized by a joint HMM-GMRF energy model and wavelet-domain supervision to ensure high-fidelity 360° recovery.

where w_i^t is the kinematic-aware weight derived from the spatio-temporal curvature (STC). This ensures that the watermark signal evolves fluidly alongside the dynamic scene geometry \mathbf{x}_i^t while strictly maintaining photometric fidelity.

Omnidirectional 360° Supervision. To enable watermark extraction from any viewing angle, we implement a dense multi-view supervision strategy during the optimization phase. We define a set of M virtual viewpoints $\mathcal{V} = \{v_j\}_{j=1}^M$, sampled at uniform angular intervals of 15° around the asset. For each timestamp t and viewpoint v_j , the rendered image $\hat{\mathcal{I}}_{v_j}^t$ must satisfy the recovery constraint:

$$\forall v_j \in \mathcal{V}, \quad \mathcal{D}(\hat{\mathcal{I}}_{v_j}^t) \approx \mathbf{B}, \quad (4)$$

where \mathcal{D} is the pre-trained neural decoder[48]. This formulation ensures that the copyright information is invariant from any observation point.

4 Methodology

This section details the theoretical modeling and mathematical derivation of our curvature-modulated HMM-MRF spatio-temporal consistent watermarking framework for 4D-GS. As shown in Figure 2, our method achieves covert and highly robust embedding of copyright information \mathcal{B} within 4D space without compromising the original rendering capabilities of 4DGS.

4.1 Kinematic Analysis of Gaussian Trajectories

In dynamic scene reconstruction, the parameter evolution of a 4D Gaussian field essentially describes the underlying motion manifold. The trajectory of a dense Gaussian \mathbf{p}_i across continuous video frames can be modeled as a continuous function of time $\mathbf{x}_i(t)$. To quantify the dynamical instability of Gaussian trajectory, we define the instantaneous velocity \mathbf{v}_i^t and acceleration \mathbf{a}_i^t :

$$\mathbf{v}_i^t = \frac{\mathbf{x}_i^t - \mathbf{x}_i^{t-1}}{\Delta t}, \quad \mathbf{a}_i^t = \frac{\mathbf{v}_i^t - \mathbf{v}_i^{t-1}}{\Delta t}. \quad (5)$$

According to classical curve geometry and motion perception theory, the instantaneous *Spatio-Temporal Curvature* (STC) κ_i^t [27] measures the intensity of changes in the magnitude and direction of the velocity vector:

$$\kappa_i^t = \frac{\|\mathbf{v}_i^t \times \mathbf{a}_i^t\|_2}{\|\mathbf{v}_i^t\|_2^3 + \epsilon}, \quad (6)$$

where ϵ is a small constant for numerical stability. Regions with high κ_i^t correspond to “Dynamic Instants” (e.g., sudden collisions or sharp turns), where the underlying parameter manifolds are highly

sensitive and fragile. And these regions are visually salient and possess fragile underlying parameter manifolds that are susceptible to damage from watermark gradients. Injecting watermark gradients into such regions tends to distort the motion semantics, leading to severe visual artifacts. To mitigate this, we introduce a geometry-aware mapping that transforms STC into a *Watermark Embedding Confidence Weight* w_i^t :

$$w_i^t = \exp\left(-\frac{\kappa_i^t}{\tau}\right) \quad (7)$$

where τ is a decay factor. This weight acts as a gating signal for gradient routing: in stable regions (e.g., low-curvature points $w_i^t \rightarrow 1$), the system allows high-SNR watermark injection, whereas in high-dynamic regions (e.g., high-curvature points $w_i^t \rightarrow 0$), it enforces physical isolation for watermark injection to preserve motion integrity. To handle the potentially large dynamic range of κ_i^t and prevent weight sparsity, we apply a mini-batch normalization to w_i^t during training, followed by a sigmoid-like clamping to ensure the weights are well-distributed within the $[0, 1]$ interval.

4.2 Spatial-Temporal Consistency via Optimal Transport

Since the watermark is extracted from 2D rendered images, the 4D Gaussian field must consistently carry watermark segments across frames to ensure robust decoding and eliminate high-frequency temporal oscillations (i.e., bit flicker). To achieve this temporal persistence while maintaining spatial coherence, we enforce a robust spatio-temporal consistency prior by modeling the evolution of the Gaussian field as a stochastic process on a dynamic random field. Standard 4D consistency constraints rely on fixed index-wise correspondences. However, during 4D-GS optimization, primitives undergo frequent densification, pruning, and resampling to maintain rendering quality, leading to topological mutations across frames. Such correspondence breakage introduces systematic bias into the consistency loss, manifesting as irregular oscillations during training.

To address this hidden-variable matching problem, we model the temporal evolution as a stochastic process. Specifically, we model the spatio-temporal states as a *Hidden Markov Model (HMM)*, where the transition prior is established via *Optimal Transport (OT)* [33, 23] to handle topological mutations. Furthermore, the spatial interactions are regularized through a *Gaussian Markov Random Field (GMRF)* to ensure neighborhood coherence.

Topological Alignment via Optimal Transport. We resolve the aforementioned correspondence ambiguity by leveraging OT theory to infer the transition prior as a hidden-variable matching problem. We treat primitive sets at adjacent timestamps as discrete measures μ_t and μ_{t-1} , and solve for the optimal transport plan γ^* via the geometry-aware entropy-regularized Wasserstein distance [30]:

$$\min_{\gamma \in \Pi(\mu_t, \mu_{t-1})} \sum_{i,j} \gamma_{ij} \|\mathbf{x}_i^t - \mathbf{x}_j^{t-1}\|_2^2 - \epsilon H(\gamma). \quad (8)$$

where $H(\gamma)$ is the entropic penalty solved efficiently via the Sinkhorn algorithm [8]. To maintain training efficiency, the OT alignment is performed on a subsampled set of keyframes and Gaussian primitives. Based on the optimal plan γ^* , we employ a **barycentric mapping** to retrieve the aligned prior state $\hat{\mathbf{z}}_i^{t-1}$ for the i -th Gaussian:

$$\hat{\mathbf{z}}_i^{t-1} = \sum_j \frac{\gamma_{ij}^*}{\sum_k \gamma_{ik}^*} \mathbf{z}_j^{t-1}, \quad (9)$$

where $\mathbf{z} = [\mathbf{x}, \mathbf{s}]^\top$ encompasses both spatial coordinates and appearance attributes. This alignment ensures that consistency regularization operates on physical motion residuals $\Delta \mathbf{z}$ rather than noise.

Gated Consistency Energy. Using the OT-aligned reference $\hat{\mathbf{z}}_i^{t-1}$, the GMRF formulation unifies temporal transitions and spatial interactions into a **Gated Consistency Loss** \mathcal{L}_{con} :

$$\mathcal{L}_{con} = \sum_i w_i^t \left(\|\mathbf{z}_i^t - \hat{\mathbf{z}}_i^{t-1}\|_2^2 + \sum_{j \in \mathcal{N}_i} \beta_{ij} \|\mathbf{z}_i^t - \mathbf{z}_j^t\|_2^2 \right). \quad (10)$$

Here, \mathcal{N}_i denotes the set of K -nearest neighbors for the i -th Gaussian, β_{ij} denotes spatial adjacency weights. As established in Sec 4.1, the kinematic weight w_i^t acts as a precision factor for this prior. It enforces a *phase-locking* mechanism in stable regions to anchor watermark bits, while adaptively relaxing constraints at ‘‘Dynamic Instants’’ to ensure that regularization operates on true physical motion residuals rather than topological noise.

4.3 Curvature-Gated Spatial-Temporal MAP Optimization

To ensure the watermark signal is embedded both persistently and coherently, we formulate the optimization as a Maximum A Posteriori (MAP) inference problem. Within this framework, the search for the optimal Gaussian states \mathcal{Z}_t is guided by the following energy functional:

$$\mathcal{E}(\mathcal{Z}t) = \mathcal{L}_{data} + \lambda_{con}\mathcal{L}_{con}(\mathcal{Z}t, \hat{\mathcal{Z}}t - 1), \quad (11)$$

where \mathcal{L}_{data} represents the other joint reconstruction and watermark decoding loss (detailed in Sec. 4.4). The term \mathcal{L}_{con} , as defined in Eq. (10), functions as a Spatial-Temporal Markov Prior. Crucially, the kinematic weight w_i^t acts as a precision factor for this prior: it enforces a *phase-locking* mechanism in dynamically stable regions ($w_i^t \rightarrow 1$) to anchor watermark bits, while adaptively relaxing constraints in ‘‘Dynamic Instants’’ ($w_i^t \rightarrow 0$). This probabilistic formulation ensures that the embedding process is not a mere perturbation but is regularized by the underlying motion manifold, providing the necessary boundary conditions for the anisotropic diffusion analyzed in Sec. C.3.

4.4 Kinematic-Aware Joint Optimization

To ensure that the embedded watermark remains robust and imperceptible within the dynamic 4D radiance field, we propose a **Kinematic-Aware joint optimization** objective.

Frequency-Domain Watermark Supervision. To enhance the robustness of information hiding while maintaining high-frequency rendering fidelity, we perform watermark extraction and supervision in the frequency domain using Discrete Wavelet Transform (DWT). For a rendered image $\hat{\mathcal{I}}_{v_j}^t$ at timestamp t from viewpoint $v_j \in \mathcal{V}$, the DWT operator Φ decomposes it into a low-frequency subband $\hat{\mathcal{I}}_{LL}$ and a set of high-frequency subbands $\hat{\mathcal{I}}_H = \{\hat{\mathcal{I}}_{LH}, \hat{\mathcal{I}}_{HL}, \hat{\mathcal{I}}_{HH}\}$ based on $[\hat{\mathcal{I}}_{LL}, \hat{\mathcal{I}}_H] = \Phi(\hat{\mathcal{I}}_{v_j}^t)$.

Kinematic-Aware Watermark Message Loss: The L -bit watermark \mathbf{B} is decoded exclusively from the stable $\hat{\mathcal{I}}_{LL}$ component. We employ a pre-trained message decoder \mathcal{D} followed by a sigmoid function $\sigma(\cdot)$ to extract the message $\hat{\mathbf{B}} = \sigma(\mathcal{D}(\hat{\mathcal{I}}_{LL}))$ within the range of $[0, 1]$. The watermark message loss \mathcal{L}_{wm} is defined as the Binary Cross Entropy (BCE) between $\hat{\mathbf{B}}$ and the ground truth \mathbf{B} :

$$\mathcal{L}_{wm} = - \sum_{i=1}^N (\mathbf{B}_i \log(\hat{\mathbf{B}}_i) + (1 - \mathbf{B}_i) \log(1 - \hat{\mathbf{B}}_i)). \quad (12)$$

Wavelet-subband Loss. To prevent the watermark embedding degrading high-frequency structural details, we follow [12] to adopt wavelet-subband loss \mathcal{L}_{wav} . This loss enforces consistency between the high-frequency coefficients of the watermarked image and the ground truth image \mathcal{I}^{gt} :

$$\mathcal{L}_{wav} = \sum_l \sum_{s \in \mathcal{H}} \mathbb{E} \left[\left\| \Phi_{s,l}(\hat{\mathcal{I}}_{v_j}^t) - \Phi_{s,l}(\mathcal{I}^{gt}) \right\|_1 \right], \quad (13)$$

where $\Phi_{s,l}(\cdot)$ is the DWT coefficients in subband s at decomposition level l .

Curvature-Modulated Joint Objective. To spatially redistribute the watermark injection intensity, we reformulate the message loss \mathcal{L}_{wm} as a kinetically-gating factor. By modulating the contribution of each Gaussian primitive to the message extraction gradient, we ensure that low-curvature points ($w_i^t \rightarrow 1$) act as high-SNR channels, while high-curvature points ($w_i^t \rightarrow 0$) suppress embedding. Finally, 4D-GSW is optimized with the total loss, which is the weighted sum of all losses:

$$\mathcal{L}_{total} = \lambda_{wm}\mathcal{L}_{wm} + \lambda_{wav}\mathcal{L}_{wav} + \lambda_{con}\mathcal{L}_{con} + \lambda_{rec}\mathcal{L}_{rec} \quad (14)$$

where $\mathcal{L}_{rec} = \mathcal{L}_{ref} + \lambda_l\mathcal{L}_{lpips} + \lambda_m\mathcal{L}_{mask} + \lambda_{ga}\mathcal{L}_{ga} + \lambda_{sds}\mathcal{L}_{sds}$ aims to maintain the structural and photometric integrity of the 4D asset. Specifically, \mathcal{L}_{ref} ensures photometric fidelity, \mathcal{L}_{lpips} guarantees perceptual invisibility, \mathcal{L}_{mask} enforces geometric boundaries, and \mathcal{L}_{sds} ensures 3D-consistent geometry. \mathcal{L}_{sds} ensures 3D-consistent geometry from monocular input. \mathcal{L}_{ga} provides generative augmentation to further refine the detail synthesis in occluded regions. More loss details can refer to [37]. By concentrating the curvature-based gating w_i^t exclusively on the watermarking terms, our framework induces an *anisotropic gradient routing* mechanism. This allows the model to ‘‘bake’’ information into stable radiance manifolds without interfering with the complex motion optimization handled by the foundational losses, effectively preventing ‘‘FVD collapse’’.

Kinematic-Aware Anisotropic Gradient Routing. A naive optimization of Eq. (15) would uniformly distribute the watermark gradients across all Gaussian primitives, inevitably disrupting fragile motion trajectories and leading to ‘‘FVD collapse’’. To physically decouple the watermark embedding from complex scene dynamics, we implement a an *anisotropic gradient routing* mechanism.

Specifically, during backpropagation, the gradients of the watermark-related and consistency losses flowing into the appearance attribute (i.e., the 0-th order DC component s_i^t) of the i -th Gaussian are element-wise modulated by the kinematic weight w_i^t :

$$\frac{\partial \mathcal{L}_{total}}{\partial s_i^t} = \underbrace{\frac{\partial \mathcal{L}_{rec}}{\partial s_i^t}}_{\text{Reconstruction}} + w_i^t \cdot \underbrace{\frac{\partial (\lambda_{wm} \mathcal{L}_{wm} + \lambda_{wav} \mathcal{L}_{wav} + \lambda_{con} \mathcal{L}_{con})}{\partial s_i^t}}_{\text{Selective Embedding}} \quad (15)$$

This asymmetric distribution of optimization pressure ensures that high-curvature primitives ($w_i^t \rightarrow 0$), which are critical for motion realism, naturally suppress watermark embedding. Conversely, dynamically stable primitives ($w_i^t \rightarrow 1$) receive strong watermark gradients. This gradient-level gating directly implements the anisotropic diffusion prior defined in Sec 4.2, isolating watermark-induced perturbations from non-rigid deformations.

5 Experiments

Dataset and Metrics. We evaluate on the Consistent4D dataset [13], utilizing seven animated assets for quantitative analysis and real-world monocular videos for qualitative validation. Following standard protocols, we reconstruct scenes from a monocular view and evaluate Novel View Synthesis (NVS) on four unseen views. To comprehensively assess the 4D assets [37, 9, 18, 17], we report PSNR and SSIM [35] (photometric fidelity), LPIPS [45] (perceptual quality), CLIP score [26] (semantic consistency), and Fréchet Video Distance (FVD) [32] (temporal realism) to quantify the distribution shift in the I3D [4] feature space.

Implementation Details. We instantiate our framework on the Sparse-Controlled 4D-GS (SC4D) backbone [37], where N dense Gaussians are driven by a sparse set of control points ($M \approx 512$) via Linear Blend Skinning (LBS). While SC4D ensures local geometric rigidity, our kinematic-aware constraints specifically regularize the temporal smoothness of the appearance carrier s_i^t against watermark-induced high-frequency noise. Our message decoder architecture is consistent with that of HiDDeN [48] and equipped with fine-tuned pre-trained weights. We implemented our framework in PyTorch, training each scene for 10,000 iterations (~ 1 hour) on a single NVIDIA RTX A6000 GPU.

5.1 Quantitative Comparison

Table 1: Quantitative comparison on dynamic scene reconstruction and watermarking.

Methods	PSNR \uparrow	SSIM \uparrow	LPIPS \downarrow	CLIP \uparrow	FVD \downarrow
Consistent4D [13]	27.62	0.89	0.132	0.908	1518.56
4DGen [41]	21.80	0.90	0.130	0.894	-
4Diffusion [44]	-	-	0.228	0.873	1551.63
L4GM [28]	21.80	0.90	0.158	0.913	1360.04
SC4D [37]	27.67	0.89	0.139	0.911	1297.18
SC4D[37] + HiDDeN[48]	27.08	0.89	0.155	0.880	1601.50
SC4D[37] + 3D-GSW[12]	23.31	0.84	0.206	0.815	1820.50
4D-GSW (Ours)	28.36	0.91	0.133	0.904	1331.19

Reconstruction Fidelity and Temporal Consistency. As shown in Table 1, **4D-GSW** consistently outperforms the watermarking baseline across most metrics. Detailed per-sample results refer to Table 4 in Appendix. Critically, while naive 2D watermark integration causes a severe FVD spike (from 1297.18 to 1601.50) due to temporal flickering, our method maintains a competitive FVD of 1331.19. This minimal overhead validates the efficacy of our *anisotropic gradient routing* in preserving motion physics. Furthermore, 4D-GSW achieves superior PSNR and SSIM, even surpassing the non-watermarked SC4D. We attribute this to the HMM-MRF energy model, which provides a structured spatio-temporal prior that regularizes the underlying radiance field. While L4GM [28] yields a higher CLIP score via generative priors, our framework strikes a better balance between photometric fidelity and motion realism, successfully "baking" robust copyright information into 4D assets with negligible quality degradation.

Robustness against Visual Distortions. We evaluate the bit accuracy of **4D-GSW** under various simulated attacks to verify its reliability. As shown in Table 2, our method achieves a superior average accuracy of **98.05%**, consistently outperforming the baseline. Detailed per-sample results refer to Table 5 in Appendix. Specifically, 4D-GSW reaches **99.10%** accuracy under the "None"

Table 2: Robustness evaluation against various distortions. We report the bit accuracy of the extracted watermark (a 48-bit string) across different attack scenarios.

Methods	None	Noise ($\mu=0.1$)	Rotation ($\pm\pi/6$)	Scaling ($\leq 25\%$)	Blur ($\sigma=0.1$)	Crop (20%)	Resize (0.9~1.0)	JPEG (50% quality)	Average
SC4D[37] + HiDDeN[48]	97.33	94.01	94.27	94.14	94.60	94.92	95.44	93.23	94.74
SC4D[37] + 3D-GSW[12]	97.28	94.85	82.18	97.40	97.25	96.36	97.37	97.35	95.01
4D-GSW (Ours)	99.10	96.84	98.65	97.97	97.94	98.00	97.98	97.89	98.05

setting, benefiting from our *Topology-Aware Consistency Model* which stabilizes the watermark signal within the 4D radiance field. Our framework also exhibits remarkable resilience to geometric transformations, maintaining over **97.9%** accuracy under severe rotation and scaling. This is attributed to our omnidirectional supervision and DC-component embedding, which ensure viewpoint invariance. Furthermore, our method remains robust against high-frequency information loss (e.g., JPEG compression and cropping), staying above **97.8%**. These results validate that our *anisotropic diffusion* creates a redundant, robust representation across stable manifolds that is highly resistant to both local and global distortions.

Table 3: Ablation study of different components in 4D-GSW.

Methods	PSNR \uparrow	SSIM \uparrow	LPIPS \downarrow	CLIP \uparrow	FVD \downarrow	ACC \uparrow
w/o temporal	26.34	0.87	0.16	0.85	1825.70	94.60
w/o spatial	25.21	0.88	0.17	0.87	1688.47	96.84
w/o curvature	26.12	0.90	0.15	0.88	1491.14	96.21
4D-GSW (Ours)	28.36	0.91	0.133	0.904	1331.19	99.10

Ablation Study. Table 3 validates the contribution of our core components. 1) *Temporal Consistency*: Removing the OT-aligned HMM prior (**w/o temporal**) causes severe ‘‘FVD collapse’’ (1825.70) and drops ACC to 94.60%, proving that temporal phase-locking is essential for both motion realism and decoding robustness. 2) *Spatial Regularization*: Disabling the GMRF prior (**w/o spatial**) degrades PSNR to 25.21 dB, confirming that spatial affinity is critical for smooth signal distribution along the radiance manifold. 3) *Curvature Gating*: Excluding STC-based gradient routing (**w/o curvature**) spikes FVD to 1491.14, demonstrating the necessity of shielding dynamic instants to prevent trajectory distortion. Overall, the full **4D-GSW** achieves the optimal fidelity-robustness trade-off, confirming that our anisotropic optimization decouples watermark embedding from complex 4D scene geometry.

5.2 Qualitative Results

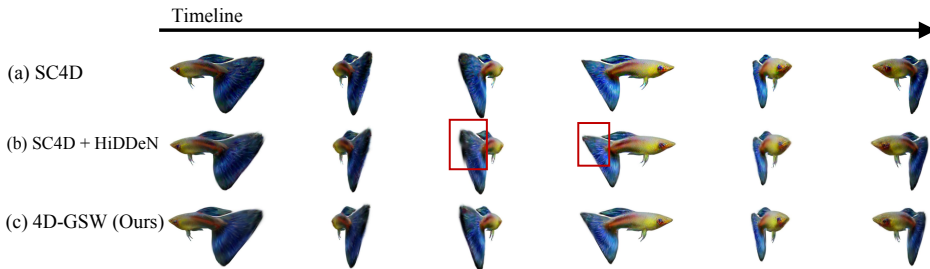


Figure 3: **Visualization of temporal consistency on the Guppie sequence.** The baseline (b) suffers from severe temporal flickering and geometric jitter during rapid motion (red boxes). In contrast, our **4D-GSW** (c) maintains high structural integrity and motion smoothness consistent with the baseline.

1) *Spatio-Temporal and Cross-View Consistency*: As shown in Fig. 3 and Fig. 5, the **SC4D+HiDDeN** baseline suffers from severe temporal flickering, geometric jitter, and structural drift across novel views, indicating an ‘‘FVD collapse.’’ In contrast, **4D-GSW** generates smooth, coherent dynamics and maintains stable 3D geometric structures from arbitrary viewpoints. By leveraging the Kinematic-Aware Gating mechanism, our framework effectively shields fragile motion segments from non-physical perturbations.

2) *Photometric Fidelity and Anisotropic Error Distribution*: Fig. 6 compares reconstruction details. While the baseline blurs structural boundaries (e.g., *Pistol* contours, *Rose* petals) and scatters stochastic errors across critical geometries, **4D-GSW** preserves sharp, fine-grained details consistent with

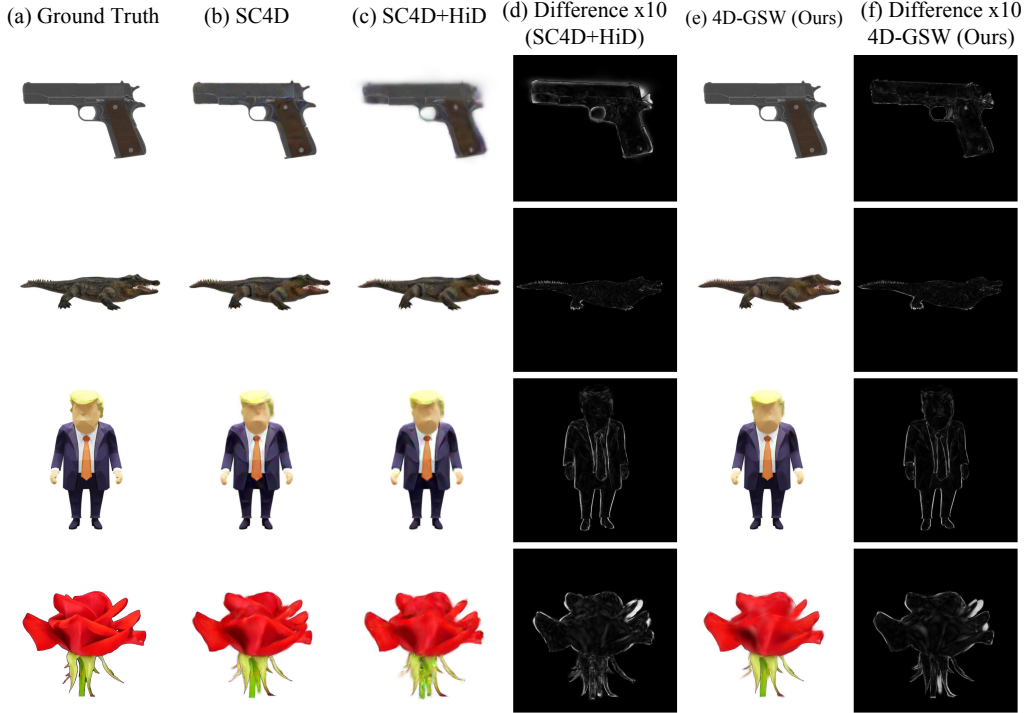


Figure 4: **Visualization across diverse dynamic assets.** Comparison of models generated by SC4D, SC4D+Hidden, and our method across different viewpoints at the same time step.

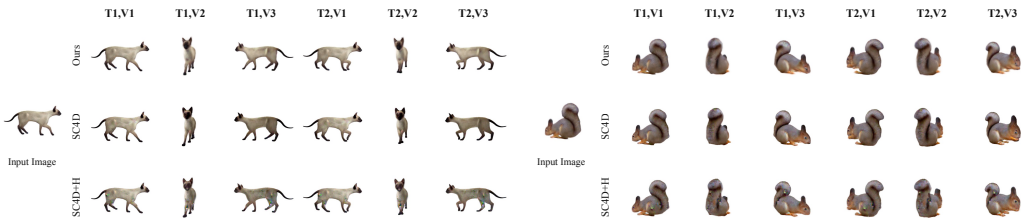


Figure 5: **Multi-view 4D Generation Results at Different Timestamps.** Comparison of models generated by SC4D [37], SC4D+Hidden [48], and our method across different viewpoints at the different timestep.

the Ground Truth. Furthermore, the $10\times$ residual maps visually confirm our anisotropic gradient routing: the watermark signal is adaptively concentrated in stable, texture-rich regions and repelled from motion-sensitive edges, achieving an optimal trade-off between robustness and imperceptibility.

6 Conclusion

In this paper, we presented **4D-GSW**, a kinematic-aware watermarking framework for 4D Gaussian Splatting. To address the temporal artifacts induced by naive frame-wise embedding, we introduce a Spatio-Temporal Curvature (STC) metric that adaptively gates watermark gradients, shielding sensitive dynamic instants from non-physical perturbations. By formulating the embedding process as a joint HMM-MRF optimization regularized by Optimal Transport, our method successfully handles topological mutations to maintain rigorous spatio-temporal consistency. Rather than arbitrary injection, this curvature-gated mechanism acts as an anisotropic structural regularizer, effectively embedding robust copyright information into stable radiance manifolds. Extensive evaluations demonstrate that 4D-GSW achieves high resilience against diverse distortions with minimal degradation to motion realism, providing a practical foundation for IP protection in dynamic neural rendering.

Discussion and Limitations. Our STC metric assumes C^2 continuous Gaussian trajectories. During extreme non-rigid events (e.g., topological fracturing), this continuity is violated, rendering the kinematic manifold non-differentiable. Consequently, localized oscillations in the embedding weight

w_i^t can weaken the diffusion barrier, marginally degrading watermark robustness in these singular regions. Addressing such stochastic dynamics remains an avenue for future work.

Acknowledgments and Disclosure of Funding

We thank our colleagues and collaborators for insightful discussions, careful feedback, and support throughout this project. We are grateful to the developers and maintainers of the open-source models, libraries, and evaluation tools that made our experiments possible. We hope that we have provided meaningful insight into the future development of image generation and editing models.

References

- [1] Jeongmin Bae, Seoha Kim, Youngsik Yun, Hahyun Lee, Gun Bang, and Youngjung Uh. Per-gaussian embedding-based deformation for deformable 3d gaussian splatting. In *European Conference on Computer Vision (ECCV)*, 2024.
- [2] Jonathan T Barron, Ben Mildenhall, Matthew Tancik, Peter Hedman, Ricardo Martin-Brualla, and Pratul P Srinivasan. Mip-nerf: A multiscale representation for anti-aliasing neural radiance fields. In *Proceedings of the IEEE/CVF International Conference on Computer Vision*, pages 5855–5864, 2021.
- [3] Jonathan T Barron, Ben Mildenhall, Dor Verbin, Pratul P Srinivasan, and Peter Hedman. Zip-NeRF: Anti-aliased grid-based neural radiance fields. In *Proceedings of the IEEE/CVF International Conference on Computer Vision*, pages 19697–19705, 2023.
- [4] Joao Carreira and Andrew Zisserman. Quo vadis, action recognition? a new model and the kinetics dataset. In *proceedings of the IEEE Conference on Computer Vision and Pattern Recognition*, pages 6299–6308, 2017.
- [5] Jianing Chen, Zehao Li, Yujun Cai, Hao Jiang, Chengxuan Qian, Juyuan Kang, Shuqin Gao, Honglong Zhao, Tianlu Mao, and Yucheng Zhang. HAIF-GS: Hierarchical and induced flow-guided gaussian splatting for dynamic scene. In *The Thirty-ninth Annual Conference on Neural Information Processing Systems*, 2025.
- [6] Yiwen Chen, Zilong Chen, Chi Zhang, Feng Wang, Xiaofeng Yang, Yikai Wang, Zhongang Cai, Lei Yang, Huaping Liu, and Guosheng Lin. Gaussianeditor: Swift and controllable 3d editing with gaussian splatting. In *CVPR*, 2024.
- [7] Zixuan Chen, Guangcong Wang, Jiahao Zhu, Jianhuang Lai, and Xiaohua Xie. Guardsplat: Efficient and robust watermarking for 3d gaussian splatting. In *Proceedings of the IEEE/CVF Conference on Computer Vision and Pattern Recognition (CVPR)*, pages 16325–16335, 2025.
- [8] Marco Cuturi. Sinkhorn distances: Lightspeed computation of optimal transport. *Advances in neural information processing systems*, 26, 2013.
- [9] Yijia Guo, Wenkai Huang, Yang Li, Gaolei Li, Hang Zhang, Liwen Hu, Jianhua Li, Tiejun Huang, and Lei Ma. Splats in splats: Robust and effective 3d steganography towards gaussian splatting. In *AAAI*, 2026.
- [10] Pengchong Hu and Zhizhong Han. Vtgaussian-slam: Rgb-d slam for large scale scenes with splatting view-tied 3d gaussians. In *Proceedings of the 42nd International Conference on Machine Learning*, 2025.
- [11] Youngdong Jang, Seungwoo Bae, Jaekyung Kim, and Sangpil Yu. Waterf: Robust watermarks in radiance fields for protection of copyrights. In *IEEE/CVF Conference on Computer Vision and Pattern Recognition (CVPR)*, 2025.
- [12] Youngdong Jang, Hyunje Park, Feng Yang, Heeju Ko, Euijin Choo, and Sangpil Kim. 3d-gsw: 3d gaussian splatting for robust watermarking. In *Proceedings of the IEEE/CVF Conference on Computer Vision and Pattern Recognition (CVPR)*, pages 5938–5948, 2025.
- [13] Yanqin Jiang, Li Zhang, Jin Gao, Weiming Hu, and Yao Yao. Consistent4d: Consistent 360° dynamic object generation from monocular video. In *The Twelfth International Conference on Learning Representations*, 2024.
- [14] Yuheng Jiang, Zehao Shen, Penghao Wang, Zhuo Su, Yu Hong, Yingliang Zhang, Jingyi Yu, and Lan Xu. Hifi4g: High-fidelity human performance rendering via compact gaussian splatting. In *Proceedings of the IEEE/CVF Conference on Computer Vision and Pattern Recognition (CVPR)*, pages 19734–19745, June 2024.
- [15] Bernhard Kerbl, Georgios Kopanas, Thomas Leimkühler, and George Drettakis. 3d gaussian splatting for real-time radiance field rendering. *ACM Transactions on Graphics*, 2023.

- [16] Chenxin Li, Brandon Y. Feng, Zhiwen Fan, Panwang Pan, and Zhangyang Wang. Steganerf: Embedding invisible information within neural radiance fields. In *Proceedings of the IEEE/CVF International Conference on Computer Vision (ICCV)*, 2023.
- [17] Hanzhi Li, Wenkang Li, Wenbo Hu, Kaidong Zhang, Yifan Zhao, Yuewen Liu, Yong Liu, and Boxin Wen. Gaussianmarker: Uncertainty-aware copyright protection of 3d gaussian splatting. In *Proceedings of the 32nd ACM International Conference on Multimedia*, pages 2500–2509, 2024.
- [18] Hengyu Liu, Chenxin Li, Wentao Pan, Zhiqin Yang, Yifeng Yang, Yifan Liu, Wuyang Li, and Yixuan Yuan. Hide-in-motion: Embedding steganographic copyright information into 4d gaussian splatting assets. In *2025 IEEE International Conference on Robotics and Automation (ICRA)*, pages 2694–2700, 2025.
- [19] Yifan Liu, Chenxin Li, Hengyu Liu, Chen Yang, and Yixuan Yuan. Foundation model-guided gaussian splatting for 4d reconstruction of deformable tissues. *IEEE Transactions on Medical Imaging*, 2025.
- [20] Jonathon Luiten, Georgios Kopanas, Bastian Leibe, and Deva Ramanan. Dynamic 3d gaussians: Tracking by persistent dynamic view synthesis. In *3DV*, 2024.
- [21] Ziyuan Luo, Qing Guo, Ka Chun Cheung, Simon See, and Renjie Wan. CopyRNeRF: Protecting the copyright of neural radiance fields. In *Proceedings of the IEEE/CVF International Conference on Computer Vision*, 2023.
- [22] Ben Mildenhall, Pratul P Srinivasan, Matthew Tancik, Jonathan T Barron, Ravi Ramamoorthi, and Ren Ng. NeRF: Representing scenes as neural radiance fields for view synthesis. In *European Conference on Computer Vision*, pages 405–421. Springer, 2020.
- [23] Eduardo Fernandes Montesuma, Fred Maurice Ngolè Mboula, and Antoine Souloumiac. Recent advances in optimal transport for machine learning. *IEEE Transactions on Pattern Analysis and Machine Intelligence*, 47(2):1161–1180, 2025.
- [24] Keunhong Park, Utkarsh Sinha, Jonathan T. Barron, Sofien Bouaziz, Dan B Goldman, Steven M. Seitz, and Ricardo Martin-Brualla. Nerfies: Deformable neural radiance fields. *ICCV*, 2021.
- [25] Albert Pumarola, Enric Corona, Gerard Pons-Moll, and Francesc Moreno-Noguer. D-NeRF: Neural Radiance Fields for Dynamic Scenes. In *Proceedings of the IEEE/CVF Conference on Computer Vision and Pattern Recognition*, 2021.
- [26] Alec Radford, Jong Wook Kim, Chris Hallacy, Aditya Ramesh, Gabriel Goh, Sandhini Agarwal, Girish Sastry, Amanda Askell, Pamela Mishkin, Jack Clark, et al. Learning transferable visual models from natural language supervision. In *ICML*, 2021.
- [27] Cen Rao, Alper Yilmaz, and Mubarak Shah. View-invariant representation and recognition of actions. *International journal of computer vision*, 50(2):203–226, 2002.
- [28] Jiawei Ren, Kevin Xie, Ashkan Mirzaei, hanxue liang, Xiaohui Zeng, Karsten Kreis, Ziwei Liu, Antonio Torralba, Sanja Fidler, Seung Wook Kim, and Huan Ling. L4GM: Large 4d gaussian reconstruction model. In *The Thirty-eighth Annual Conference on Neural Information Processing Systems*, 2024.
- [29] Sara Fridovich-Keil and Giacomo Meanti, Frederik Rahbæk Warburg, Benjamin Recht, and Angjoo Kanazawa. K-planes: Explicit radiance fields in space, time, and appearance. In *CVPR*, 2023.
- [30] Justin Solomon, Fernando De Goes, Gabriel Peyré, Marco Cuturi, Adrian Butscher, Andy Nguyen, Tao Du, and Leonidas Guibas. Convolutional wasserstein distances: Efficient optimal transportation on geometric domains. *ACM Transactions on Graphics (ToG)*, 34(4):1–11, 2015.
- [31] Yuqi Tan, Xiang Liu, Shuzhao Xie, Bin Chen, Shu-Tao Xia, and Zhi Wang. Water-gs: Toward copyright protection for 3d gaussian splatting via universal watermarking, 2024.

- [32] Thomas Unterthiner, Sjoerd van Steenkiste, Karol Kurach, Raphaël Marinier, Marcin Michalski, and Sylvain Gelly. FVD: A new metric for video generation, 2019.
- [33] Cédric Villani et al. *Optimal transport: old and new*, volume 338. Springer, 2009.
- [34] Cong Wang, Di Kang, Heyi Sun, Shenhan Qian, Zixuan Wang, Linchao Bao, and Song-Hai Zhang. Mega: Hybrid mesh-gaussian head avatar for high-fidelity rendering and head editing. In *Proceedings of the IEEE/CVF Conference on Computer Vision and Pattern Recognition (CVPR)*, pages 26274–26284, June 2025.
- [35] Zhou Wang, Alan C. Bovik, Hamid R. Sheikh, and Eero P. Simoncelli. Image quality assessment: From error visibility to structural similarity. *IEEE Transactions on Image Processing*, 13(4):600–612, 2004.
- [36] Guanjun Wu, Taoran Yi, Jiemin Fang, Lingxi Xie, Xiaopeng Zhang, Wei Wei, Wenyu Liu, Qi Tian, and Xinggang Wang. 4d gaussian splatting for real-time dynamic scene rendering. In *Proceedings of the IEEE/CVF Conference on Computer Vision and Pattern Recognition (CVPR)*, 2024.
- [37] Zijie Wu, Chaohui Yu, Yanqin Jiang, Chenjie Cao, Fan Wang, and Xiang Bai. Sc4d: Sparse-controlled video-to-4d generation and motion transfer. In *European Conference on Computer Vision*, 2024.
- [38] Yunzhi Yan, Haotong Lin, Chenxu Zhou, Weijie Wang, Haiyang Sun, Kun Zhan, Xianpeng Lang, Xiaowei Zhou, and Sida Peng. Street gaussians: Modeling dynamic urban scenes with gaussian splatting. In *ECCV*, 2024.
- [39] Zeyu Yang, Hongye Yang, Zijie Pan, and Li Zhang. Real-time photorealistic dynamic scene representation and rendering with 4d gaussian splatting. In *International Conference on Learning Representations (ICLR)*, 2024.
- [40] Ziyi Yang, Xinyu Gao, Wen Zhou, Shaohui Jiao, Yuqing Zhang, and Xiaogang Jin. Deformable 3d gaussians for high-fidelity monocular dynamic scene reconstruction. *CVPR*, 2023.
- [41] Yuyang Yin, Dejia Xu, Zhangyang Wang, Yao Zhao, and Yunchao Wei. 4dgen: Grounded 4d content generation with spatial-temporal consistency. 2023.
- [42] Innfarn Yoo, Huiwen Chang, Xiyang Luo, Ondrej Stava, Ce Liu, Peyman Milanfar, and Feng Yang. Deep 3d-to-2d watermarking: Embedding messages in 3d meshes and extracting them from 2d renderings. In *2022 IEEE/CVF Conference on Computer Vision and Pattern Recognition (CVPR)*, 2022.
- [43] Haiming Zhang, Yiyao Zhu, Wending Zhou, Xu Yan, Yingjie CAI, Bingbing Liu, Shuguang Cui, and Zhen Li. SQS: Enhancing sparse perception models via query-based splatting in autonomous driving. In *The Thirty-ninth Annual Conference on Neural Information Processing Systems*, 2025.
- [44] Haiyu Zhang, Xinyuan Chen, Yaohui Wang, Xihui Liu, Yunhong Wang, and Yu Qiao. 4diffusion: Multi-view video diffusion model for 4d generation. In *The Thirty-eighth Annual Conference on Neural Information Processing Systems*, 2024.
- [45] Richard Zhang, Phillip Isola, Alexei A Efros, Eli Shechtman, and Oliver Wang. The unreasonable effectiveness of deep features as a perceptual metric. In *CVPR*, 2018.
- [46] Xuanyu Zhang, Jiarui Meng, Runyi Li, Zhipei Xu, Yongbing Zhang, and Jian Zhang. Gs-hider: Hiding messages into 3d gaussian splatting. In *Advances in Neural Information Processing Systems*, 2024.
- [47] Xuanyu Zhang, Jiarui Meng, Zhipei Xu, Shuzhou Yang, Yanmin Wu, Ronggang Wang, and Jian Zhang. SecureGS: Boosting the security and fidelity of 3d gaussian splatting steganography. In *The Thirteenth International Conference on Learning Representations*, 2025.
- [48] Jiren Zhu, Russell Kaplan, Justin Johnson, and Li Fei-Fei. Hidden: Hiding data with deep networks. In Vittorio Ferrari, Martial Hebert, Cristian Sminchisescu, and Yair Weiss, editors, *Computer Vision – ECCV 2018*, pages 682–697, Cham, 2018. Springer International Publishing.

A Impact Statement

The rapid advancement of 4D Gaussian Splatting (4DGS) has significantly lowered the barrier to creating high-fidelity dynamic digital assets, accelerating developments in virtual reality (VR), telepresence, and autonomous driving simulations. However, this accessibility exacerbates the risks of intellectual property (IP) theft, malicious manipulation, and unauthorized redistribution of 3D/4D digital replicas. Our proposed 4D-GSW framework addresses this critical vulnerability by providing a robust, kinematic-aware watermarking solution. By seamlessly baking copyright information into the underlying motion manifolds without compromising spatio-temporal realism, our work safeguards the rights of digital creators. This reliable authentication mechanism fosters a secure and sustainable ecosystem for sharing and commercializing 4D content, thereby incentivizing further innovation in the creator economy and metaverse applications.

Despite its positive intentions for IP protection, we acknowledge the dual-use nature inherent in steganographic technologies. High-capacity and visually imperceptible information hiding could theoretically be exploited by malicious actors for covert communication or embedding illicit payloads within seemingly innocuous 4D assets. Furthermore, the integration of complex spatio-temporal regularizations—such as Optimal Transport alignment and Markov Random Fields—introduces additional computational overhead during the optimization phase. This marginally increases the energy consumption and carbon footprint associated with asset generation. Future research must balance these trade-offs by exploring lightweight embedding protocols and developing corresponding 4D steganalysis countermeasures to mitigate potential security risks.

B Related Work

Dynamic 3D Scene Representations and 4DGS. While dynamic Neural Radiance Fields (NeRFs) [2, 3, 22, 25, 24] achieve high-fidelity novel view synthesis via deformation networks, their immense computational cost limits practical deployment. To address this, 3D Gaussian Splatting (3DGS) [15] enables real-time rendering via explicit point-based representations. Its temporal extensions (4DGS) [1, 40, 19] further model dynamic scenes. However, dense trajectory prediction per frame often induces optimization artifacts [36]. Alternatively, the Sparse-Controlled 4DGS (SC4D) framework [37] decouples appearance and motion by driving dense Gaussians with a minimal set of sparse control points via Linear Blend Skinning (LBS), achieving superior local rigidity and spatio-temporal fidelity. Despite these reconstructive advances, the intellectual property (IP) protection of 4DGS assets remains largely unexplored. A core challenge is ensuring watermark imperceptibility across complex spatio-temporal domains. Human visual perception is highly sensitive to abrupt motion discontinuities, which can be mathematically localized using Spatio-Temporal Curvature (STC) [27]—a metric characterizing the misalignment between velocity and acceleration. Since perturbations in high-STC regions easily trigger visible artifacts, naive frame-wise watermark injection is inadequate. Motivated by this, we build upon the efficient SC4D baseline and introduce motion-aware priors, utilizing STC to guide robust and imperceptible 4D copyright embedding.

Digital Watermarking in Neural Rendering. Neural rendering watermarking has evolved from hiding data in implicit NeRF weights [21, 16] to more sophisticated strategies for explicit 3DGS representations. Existing 3DGS schemes primarily focus on: (i) modulating Spherical Harmonic (SH) coefficients with cross-modal priors or encryption [7, 9]; (ii) strategic densification in high-uncertainty or high-frequency regions [17, 12]; and (iii) incorporating 3D distortion layers during training for geometric robustness [31]. However, applying these static methods frame-by-frame to 4DGS induces severe temporal discontinuity. While Hide-in-Motion [18] introduces 4D steganography via composite attributes, it relies on opacity heuristics and lacks explicit modeling of motion kinematics. This neglect of the underlying physical manifold leads to significant FVD degradation under complex non-rigid deformations. Furthermore, recent advancements in 3D Gaussian Splatting (3DGS) steganography and protection, such as GS-Hider [46] and SecureGS [47], have demonstrated the ability to hide large amounts of data within static scenes. Splats in Splats [9] introduced a nested structure for embedding scenes within scenes. Although these methods represent state-of-the-art performance in the 3D domain, they lack modeling of the temporal dimension. This makes it difficult to ensure temporal consistency, often leading to flickering artifacts and structural instability, and thus they cannot be directly applied to the processing of 4D assets.

C Variational Derivation of the Anisotropic Diffusion-Reaction PDE

To reveal the theoretical underpinnings of our method, we analyze the optimization objective in the continuum limit. We demonstrate that the discrete MAP energy defined in Section 3.3 converges to an anisotropic diffusion-reaction Partial Differential Equation (PDE).

C.1 The Continuous Energy Functional

We consider the watermark embedding process as a variational problem on a continuous spatio-temporal manifold $\Omega \subset \mathbb{R}^3 \times [0, T]$. Let $r(\mathbf{x}) = \mathbf{z}^t - \hat{\mathbf{z}}^{t-1}$ denote the residual state field. The total variational energy $\mathcal{E}(r)$ is formulated as:

$$\mathcal{E}(r) = \int_{\Omega} \left(\underbrace{\frac{\lambda_T}{2} |r(\mathbf{x})|^2}_{\text{Consistency Penalty}} + \underbrace{\frac{\lambda_S}{2} w(\mathbf{x}) |\nabla r(\mathbf{x})|^2}_{\text{Weighted Dirichlet Energy}} + \underbrace{\lambda_{wm} \mathcal{L}_{wm}(r)}_{\text{Source Term}} \right) d\mathbf{x} \quad (16)$$

where $w(\mathbf{x})$ is the kinematic weight derived from spatio-temporal curvature, λ_T and λ_S are the temporal and spatial regularization weights, and \mathcal{L}_{wm} is the watermark decoding loss.

C.2 Variation and the Euler-Lagrange Equation

According to the principle of least action, the optimal residual field must satisfy the condition $\delta \mathcal{E} = 0$. By introducing an infinitesimal perturbation $\eta(\mathbf{x})$ that vanishes on the boundary $\partial\Omega$, the first variation of \mathcal{E} is given by:

$$\delta \mathcal{E} = \frac{d}{d\epsilon} \mathcal{E}(r + \epsilon \eta) \Big|_{\epsilon=0} = \int_{\Omega} \left(\lambda_T r \cdot \eta + \lambda_S w \nabla r \cdot \nabla \eta + \lambda_{wm} \frac{\partial \mathcal{L}_{wm}}{\partial r} \eta \right) d\mathbf{x}. \quad (17)$$

To eliminate the gradient of the perturbation $\nabla \eta$, we apply Green's First Identity to the second term:

$$\int_{\Omega} (w \nabla r) \cdot \nabla \eta, d\mathbf{x} = \int_{\partial\Omega} \eta (w \nabla r \cdot \mathbf{n}), dS - \int_{\Omega} \eta \cdot \text{div}(w \nabla r), d\mathbf{x}. \quad (18)$$

Given that $\eta|_{\partial\Omega} = 0$, the boundary integral vanishes. Substituting this back into the variational equation, we obtain:

$$\delta \mathcal{E} = \int_{\Omega} \eta \left(\lambda_T r - \lambda_S \text{div}(w \nabla r) + \lambda_{wm} \frac{\partial \mathcal{L}_{wm}}{\partial r} \right) d\mathbf{x} = 0. \quad (19)$$

C.3 Theoretical Interpretation: Induced Anisotropic Diffusion

Since the perturbation η is arbitrary, the integrand must be zero everywhere in Ω . To provide a deeper understanding of the optimization mechanism, we analyze the objective in the continuum limit. We observe that the gradient-gated optimization in Eq. (11) encourages a steady-state behavior that aligns with an *anisotropic diffusion-reaction* process over the residual field $r(x) = z^t - \hat{z}^{t-1}$:

$$\lambda_T r(x) - \lambda_S \text{div}(D(x) \nabla r(x)) = \mathcal{G}_{wm}, \quad (20)$$

where $D(x) = \text{diag}(w(x))$ acts as a curvature-derived diffusion tensor, $\mathcal{G}_{wm} = -\lambda_{wm} \frac{\partial \mathcal{L}_{wm}}{\partial r}$ is watermark-driven source term. This formulation suggests that watermark embedding in 4D-GSW is not a random perturbation, but is regularized by a kinematics-aware prior. In stable regions, the conductance of $D(x)$ facilitates signal propagation along the manifold; conversely, in high-dynamic regions where $D(x) \rightarrow 0$, the optimization naturally penalizes sharp updates to fragile motion trajectories. This theoretical framework provides an explanation for the observed preservation of motion fidelity (Sec. 5.1) without requiring manual hyperparameter tuning for different motion scales.

Table 4: Per-sample visual quality metrics comparison. Higher PSNR, SSIM, CLIP scores and lower LPIPS, FVD indicate better visual fidelity.

Object	Method	PSNR \uparrow	SSIM \uparrow	LPIPS \downarrow	CLIP \uparrow	FVD \downarrow
Aurorus	SC4D[37] + 3D-GSW[12]	24.370	0.8804	0.1824	0.7322	2226.2
	4D-GSW (Ours)	26.683	0.9241	0.1308	0.8382	1948.23
Crocodile	SC4D[37] + 3D-GSW[12]	24.815	0.8886	0.1311	0.8544	1611.9
	4D-GSW (Ours)	26.423	0.9038	0.1116	0.8598	1688.47
Guppie	SC4D[37] + 3D-GSW[12]	22.538	0.8573	0.1630	0.8735	1014.5
	4D-GSW (Ours)	26.347	0.8978	0.1086	0.9353	764.11
Monster	SC4D[37] + 3D-GSW[12]	24.344	0.8066	0.2498	0.8065	1958.7
	4D-GSW (Ours)	29.064	0.8778	0.1769	0.9134	1286.04
Pistol	SC4D[37] + 3D-GSW[12]	20.490	0.8303	0.2311	0.7997	2358.7
	4D-GSW (Ours)	31.146	0.9299	0.0892	0.9170	1476.54
Skull	SC4D[37] + 3D-GSW[12]	24.556	0.8296	0.2431	0.8541	1978.2
	4D-GSW (Ours)	32.111	0.9090	0.1527	0.9330	1337.69
Trump	SC4D[37] + 3D-GSW[12]	22.057	0.8107	0.2389	0.7849	1595.5
	4D-GSW (Ours)	26.798	0.8926	0.1624	0.9304	817.26
Mean	SC4D[37] + 3D-GSW[12]	23.310	0.8434	0.2056	0.8151	1820.5
	4D-GSW (Ours)	28.367	0.9050	0.1332	0.9039	1331.19

C.4 Physical Interpretation

This derivation reveals that our optimization framework implicitly solves a dynamic diffusion-reaction process:

- **The Reaction Term** (λ_{Tr}): Acts as a state-retention force that prevents the watermark signal from deviating excessively from the underlying physical manifold.
- **The Diffusion Term** ($\text{div}(\mathbf{D}\nabla r)$): Represents Anisotropic Diffusion. In stable regions where $w(\mathbf{x}) \rightarrow 1$, the high conductance of $\mathbf{D}(\mathbf{x})$ facilitates the smooth propagation of watermark signals.
- **The Diffusion Barrier**: In regions of high curvature (Dynamic Instants), $\mathbf{D}(\mathbf{x}) \rightarrow 0$. This effectively creates a "barrier" that repels watermark gradients from fragile motion trajectories.

Consequently, the embedded watermark is the steady-state solution of this PDE, providing a mathematical guarantee for maintaining high FVD (Fréchet Video Distance) scores while ensuring bit accuracy.

D Detailed Quantitative Results

Refer to Table 4 and Table 5, we also provide the per-sample results for visual quality and watermark robustness evaluation.

E More Visualization Results

Fig. 6 provides a detailed view of reconstruction quality and residual distributions. Compared to the baseline which introduces blurring at structural boundaries, **4D-GSW** preserves sharp textures and fine-grained details consistent with the **Ground Truth**.

F Nomenclature

Table 5: Per-sample watermark robustness evaluation of the proposed method versus baseline across different 3D objects and attacks. We report the Bit Accuracy (BA). “Clean” refers to decoding without any attacks.

Object	Method	Clean BA \uparrow	Noise \uparrow	Rotation \uparrow	Crop \uparrow	Scaling \uparrow	Resize \uparrow	JPEG \uparrow	G. Blur \uparrow
Aurorus	SC4D[37] + 3D-GSW[12]	0.9779	0.9504	0.8267	0.9742	0.9796	0.9750	0.9763	0.9733
	4D-GSW (Ours)	0.9974	0.9688	0.9837	0.9889	0.9805	0.9805	0.9824	0.9811
Crocodile	SC4D[37] + 3D-GSW[12]	0.9521	0.9208	0.8113	0.9525	0.9588	0.9633	0.9600	0.9542
	4D-GSW (Ours)	0.9883	0.9733	0.9844	0.9857	0.9844	0.9818	0.9824	0.9831
Guppie	SC4D[37] + 3D-GSW[12]	0.9671	0.9279	0.8067	0.9588	0.9654	0.9646	0.9696	0.9688
	4D-GSW (Ours)	0.9883	0.9935	0.9772	0.9889	0.9980	0.9961	0.9980	0.9967
Monster	SC4D[37] + 3D-GSW[12]	0.9829	0.9796	0.8492	0.9650	0.9875	0.9825	0.9833	0.9838
	4D-GSW (Ours)	0.9863	0.9590	0.9967	0.9714	0.9596	0.9609	0.9635	0.9603
Pistol	SC4D[37] + 3D-GSW[12]	0.9692	0.9338	0.8008	0.9613	0.9633	0.9721	0.9654	0.9629
	4D-GSW (Ours)	0.9915	0.9427	0.9889	0.9688	0.9661	0.9720	0.9616	0.9681
Skull	SC4D[37] + 3D-GSW[12]	0.9896	0.9796	0.8329	0.9675	0.9929	0.9883	0.9863	0.9908
	4D-GSW (Ours)	0.9935	0.9492	0.9902	0.9642	0.9792	0.9785	0.9740	0.9785
Trump	SC4D[37] + 3D-GSW[12]	0.9708	0.9471	0.8250	0.9658	0.9704	0.9704	0.9738	0.9738
	4D-GSW (Ours)	0.9915	0.9928	0.9850	0.9922	0.9902	0.9889	0.9909	0.9883
Mean	SC4D[37] + 3D-GSW[12]	0.9728	0.9485	0.8218	0.9636	0.9740	0.9737	0.9735	0.9725
	4D-GSW (Ours)	0.9909	0.9684	0.9865	0.9800	0.9797	0.9798	0.9789	0.9794



Figure 6: **Visualization across diverse dynamic assets.** From left to right: (a) Ground Truth, (b) original SC4D, (c, d) SC4D+HiDDeN baseline and its $10\times$ residual map, (e, f) our **4D-GSW** and its $10\times$ residual map. While the baseline introduces blurring at structural boundaries, 4D-GSW achieves near-lossless reconstruction.

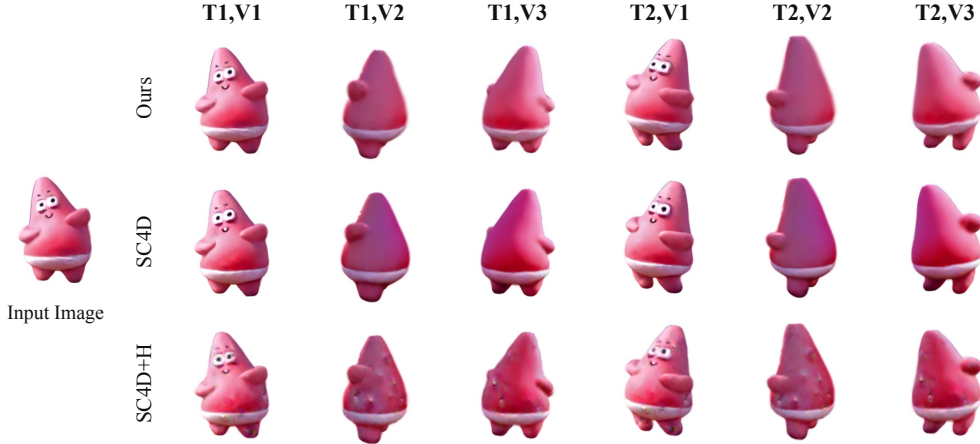


Figure 7: **Multi-view 4D generation at different timestamps.** Qualitative comparison of SC4D, SC4D+Hidden, and our method under varying viewpoints at a fixed time step.

Table 6: Nomenclature: Summary of Key Notations and Symbols.

Symbol	Description
4D Gaussian Splatting Basics	
$\mathcal{P}_t = \{\mathbf{p}_i^t\}_{i=1}^N$	Set of N Gaussian primitives at timestamp t .
$\mathbf{x}_i^t \in \mathbb{R}^3$	Geometric center position (mean) of the i -th Gaussian.
$\mathbf{s}_i^t \in \mathbb{R}^3$	Appearance state (0-th order SH / DC component).
$\mathbf{z}_i^t = [\mathbf{x}_i^t, \mathbf{s}_i^t]^\top$	Coupled spatio-temporal state vector (position and appearance).
$\alpha_i, \mathbf{q}_i, \sigma_i$	Opacity, rotation quaternion, and scaling factor, respectively.
Kinematic Analysis	
$\mathbf{v}_i^t, \mathbf{a}_i^t$	Instantaneous velocity and acceleration vectors of the i -th trajectory.
κ_i^t	Spatio-Temporal Curvature (STC) quantifying motion instability.
$w_i^t \in [0, 1]$	Curvature-derived watermark embedding confidence weight.
τ	Decay factor for the exponential mapping from STC to weight.
Spatio-Temporal Optimization	
$\gamma^*, \Pi(\cdot)$	Optimal transport plan and the set of all valid coupling measures.
$\hat{\mathbf{z}}_i^{t-1}$	OT-aligned reference state derived via barycentric mapping.
$\mathcal{N}_i, \beta_{ij}$	Spatial K -nearest neighbor set and RBF-based affinity weight.
\mathcal{L}_{con}	Gated spatio-temporal consistency loss (GMRF prior).
$\mathcal{L}_{wm}, \mathcal{L}_{wav}$	Watermark message loss (BCE) and Wavelet-subband loss.
\mathcal{L}_{rec}	Joint reconstruction loss (photometric, perceptual, and geometric).
PDE and Theoretical Modeling	
$r(\mathbf{x})$	Continuous residual field defined as $r(\mathbf{x}) = \mathbf{z}^t - \hat{\mathbf{z}}^{t-1}$.
$\mathbf{D}(\mathbf{x})$	Curvature-derived anisotropic diffusion tensor, $\text{diag}(w(\mathbf{x}))$.
\mathcal{G}_{wm}	Watermark-driven source term (gradient routing field).
λ_T, λ_S	Regularization coefficients for temporal and spatial components.
$\text{div}(\cdot), \nabla$	Divergence and gradient operators defined on the manifold.